# IV. Microdosimetry

The low energy photons considered in this work are not only slightly different from higher energy photons because of their dosimetric characteristics. They also differ in that they deposit their energy on much smaller distances than high energy photons. The secondary electrons generated in the medium, responsible for the energy deposition, induce a high number of ionization over short distances. As was already pointed out in the general introduction, this concentration of ionizations could be highly damaging for the cells. Some radiobiological and microdosimetric studies have already shown that $^{125}$I and $^{103}$Pd have indeed a RBE compared to $^{60}$Co higher than unity, which means that they are more biologically efficient than $^{60}$Co $\gamma$-rays. The precise value of the RBE however varies a lot between studies. In this work, we have investigated the mechanism of energy deposition in water vapour on different scales using two different approaches. The first is the classical microdosimetric approach where we investigate the distributions of the energy deposition events in spheres of 1 $\mu$m diameter as a function of their lineal energy y. This allows us to make a link between our work and the existing studies and the few experimental data obtained with wall-less proportional microdosimetric counters. The second approach is a cluster analysis at a nanometric scale. That scale is perhaps more representative for the mechanisms of interactions with the DNA in the nuclei. We have analysed the distribution of the clusters of ionizations as a function of their size in spheres of 2 and 10 nm radius.

The results of this study have been published in Physics in Medicine and Biology. This paper is included in page 109 and will compose the major part of this chapter.

## A. Introduction

### 1. The microdosimetric approach

Many attempts have been tried to analyse the relationship between dose and effect in radiobiology. The first ones were based on concepts like LET. They pictured the charged particle tracks as straight lines with constant energy loss or as strings of ionizations regularly or randomly spaced along the trajectory of the particle with a density that corresponds to LET. This approach has however inherent limitations as was explained in the general introduction. So more sophisticated approaches were proposed, first by Lea (1955), then later by Rossi and his co-workers who laid the theoretical and experimental foundations of microdosimetry (Rossi 1959, Rossi 1960, Rossi 1967, Rossi 1968, ICRU 36 1983). A coherent framework of concepts and quantities was proposed to quantify the statistics of energy deposition and the characteristic differences between various types of ionizing radiations.

Based on the assumption that only double strand breaks (DSB) can be really harmful for the cell, Rossi has also proposed his *Theory of Dual Radiation Action (TDRA)* (Kellerer and Rossi 1972). This theory allows to relate microdosimetry parameters to the biological effect. It assumes the assessment of Radiobiological Effect is a second-order process. The essence of the approach is to postulate the initial random products (sublesions) whose yield is proportional to energy imparted *e* and that can react pairwise. A fixed reaction probability is assumed between sublesions less than a certain distance apart. Interactions beyond this distance are disregarded. On the basis of microdosimetric data for different radiations, such assumptions can be translated into dose-response relations. One can then try to identify those sizes of the reference region that agree best with the experimental observations for substantially different radiation qualities. This approach is chosen in the first simple version of dual-action theory. It leads to the very well known linear-quadratic equation for the relation between RBE and absorbed dose.

$$e(D) = k\overline{z^2} = k(zD + D^2) \qquad \textbf{(41)}$$

where $e(D)$ is the yield of lesions at absorbed dose D and $z = z_D = \frac{1}{\bar{z}_F}\int_0^\infty z^2 f_1(z)dz$, with the subscript '1' denoting a single event distribution, is an average of specific energy *z* produced in individual events in the site.

This theory contains many simplifications and free assumptions, like the spherical shape of the sensitive region chosen rather because of the shape of the detectors used in microdosimetry than for any biological reason. The simplification is often satisfactory and sufficiently accurate to bring out the characteristic differences in the actions of various types of ionizing radiations. It has however some limitations as for the action of low-energy X-rays. For such radiations, the secondary charged particles ranges are substantially smaller than the site diameters of one or a few micrometers. Energy transfers produced by such tracks are, therefore, much more closely spaced than energy transfers randomly situated in the site. A one keV electron deposits its energy very locally in the nucleus of the cell and can thus be quite effective. This may lead to an increased biological effectiveness.

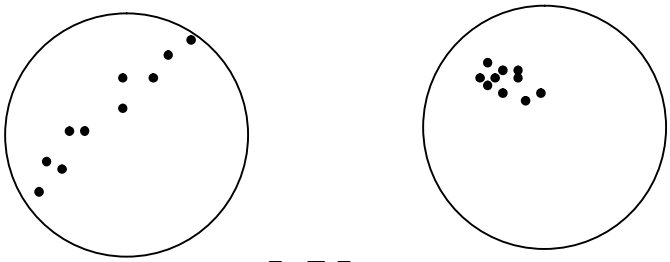


**Figure 46 : Schematic diagram of energy deposition by a particle of large range (1) and a particle of short range (2). The specific energy z is equal in the two sites, but biological effectiveness is larger for the short-range particle because of smaller distances between sublesions.**

Kellerer and Rossi have proposed a generalised formulation of the dual Radiation Action based on the existence of a sensitive matrix whose geometric characteristics are represented by the function s(x), of an energy transfer distribution characterised by the function t(x) and of a function g(x) giving the probability of interaction between sublesions (Kellerer and Rossi 1978). They obtain an equation for the average number of lesions per cell in the form of a linear-quadratic dose dependence regardless of the geometry of the sensitive matrix and of the type of radiation.

$$e(D) = k(xD + D^2)$$

where **(42)**

$$x = \int_0^\infty \frac{s(x)g(x)t(x)}{4\pi r x^2} dx \Big/ \int_0^\infty s(x)g(x)dx$$

In the case of low dose or low dose rate, the linear component (*intra*track action) dominates. On the other hand, when it is assumed that the sensitive sites are randomly dispersed over a spherical site of diameter d, and the combination probability g(x) is taken constant, as is assumed in the case of the simple TDRA, it can then be shown that $x = z$ . This leads to an equation that has been often used as a simplified way to relate microdosimetric parameters and radiobiological effectiveness, quantified by RBE. Same effect means same surviving fraction. As the surviving fraction can be written as $S(D) = e^{-ce(D)} = e^{-c(zD+D^2)}$, one can equal for low dose and/or low dose rate, for which the quadratic term can be neglected, *S(D)* with $S(D_{ref})$ and find the ratio $\frac{D_{ref}}{D} = RBE = \frac{z}{z_{ref}} = \frac{y_D}{(y_D)_{ref}}$

In a first part of this work, we have used these concepts to analyse the radiobiological effectiveness of the radiations emitted by low energy photon brachytherapy sources by comparing their $y_D$ values. The results are presented in the next article. In summary, the MS have been calculated in 1 $\mu$m diameter spheres using an event-by-event code named TRION (Lappa et al. 1993). This code allows simulating the transport of the electrons generated in a collision by a photon, and electrons down to 10 eV. It calculates too the microdosimetric parameters as the Microdosimetric Spectra (MS) and the parameters $\overline{y}_D$.

a) Description of the MC code TRION

Trion is an event-by-event Monte Carlo code. The trajectories of particles are simulated following a collision scheme, in a detailed way, where each free path and interaction with the medium has to be sampled. The approximation adopted is the gas approximation where the matter is described as separate molecules. The simulated interactions for the charged particles are the ionizations of the molecular outer shells as well as of the K-shell and the excitation of molecules. For sampling of energy transfer for ionization (McGuire 1971, Tan et al. 1978, Khare 1977), interpolation cross section constructed from the Born ionization cross section and the cross section of scattering on a free electron are used. The direction of the particles after collision is sampled after a binary collision model. For the K-shell, the movement of the electron bound to the atom and its bond with the nucleus is taken into account. The excitation of molecules by an electron is simulated according to the cross sections and mean excitation energies published by Paretzke and Berger (Paretzke 1978). The simulation of the elastic scattering of electrons is based on the Rutherford cross section including a correction term due to Molière (1948). Below 20 keV, a modified screening parameter is used (Berger).

For photons, the probability of photoionization from the atomic inner shell is assumed to be equal to 1. The photoelectron energy is calculated by the energy conservation law. Its direction is generated from the Sauter distribution (Sauter 1931). The total photoionization cross section is determined experimentally (Veigele 1973). It is assumed that K-shell ionization causes emission of an Auger electron. Its direction is assumed to be isotropic and its energy is determined using ionization potentials of outer and K-shells. Finally, the photon energy after Compton scattering is evaluated according to the Klein-Nishina cross section. Particles directions and electron energy are calculated by the conservation laws.

The results obtained using those cross section data have been compared to experimental results (Lappa et al. 1993). For electrons, which are the particles of interrest in our case, the calculated stopping powers agree very well with the measured values in water vapour and liquid water for electrons above 1keV. They are within the experimental uncertainties for

electrons below 100 eV. These experimental uncertainties are quite high for low energy electrons which makes it impossible to distinguish water vapour from liquid water. Therefore, we can conclude that the gas approximation does not introduce a supplementary error. It is, however, an approximation that could introduce a bias in the results as the energy needed to produce a pair electron-ion in liquid is much lower than for the vapour, the number of ionization therefore is underestimated by our method. But, as will be discussed later, we should keep in mind that liquid water itself is an approximation for living tissue. At this very small scale, to be correct, we should analyse the interaction with DNA molecules and not water. This kind of study is then a first step to understand the mechanism of interaction between radiation and matter at a very small scale in a very well-known and very simple medium.

TRION permits to calculate, starting from only the electron spectrum in the sensitive region, the distribution function $y$ and its moments $y^{(n)}$ for $n$ = 0, 1 and 2 of the absorbed energy in spherical or cylindrical regions under condition of electronic equilibrium in the absorber irradiated by electrons or gamma-rays using the Fluctuation Detector Method (Lappa et al. 1993, Lappa 1984, Lappa et al. 1988). The case $n$=0 is the probability that a primary particle realizes an energy absorption event Q, $P = P\{Q > 0\} = y^{(0)}$, and the cases $n$=1 and $n$=2 are the two first moments $\overline{Q} = y^{(1)}$ and $\overline{Q^2} = y^{(2)}$. Starting from those results, it is possible to calculate microdosimetric characteristics like the frequency mean lineal energy and the dose-mean lineal energy:

$$\bar{y}_F = \overline{Q}/\bar{l}P \text{ and } \bar{y}_D = \overline{Q^2}/\bar{l}\overline{Q}$$

where $\bar{l}$ is the average cord of a sphere of radius r.

The basic assumption in that method is that the process is Markovian; the interaction between particles is negligible. The site dimensions are assumed to be small compared to the typical distances in which the particle fluence changes significantly. In addition at least one of the following assumptions is assumed correct:

- the site is sphere.
- the site is oriented randomly and isotropically.
- the radiation fluence is isotropic.

b) Summary of the results (see p 145)

The situation of low energy X-rays is still an open question. It is certain that the ionization density of these X-rays is higher than for photons of higher energy as those of $^{60}$Co γ rays. We have calcultated their microdosimetric spectra, they are in the region between 1 and 10 keV/μm.

The MS and the parameter $\bar{y}_D$ have been computed for the photon spectra emitted by the IBt $^{125}$I and $^{103}$Pd seeds for different distances from the sources in water. The MS and $\bar{y}_D$ calculated for 1 cm in water for both isotopes is consistent with the very few data from the literature (Wuu et al. 1996). For $^{103}$Pd, $\bar{y}_D$ was found to be 4.05 keV/µm against 3.8 keV/µm in literature and for $^{125}$I $\bar{y}_D$ was found to be 3.6 keV/µm against 3.5 keV/µm in literature.

The initial spectrum of $^{125}$I is composed of photons energies of 27, 31 and 35 keV, the spectrum of $^{103}$Pd is composed of three photon energies around 20 keV but also of a gamma emission of 357 keV of a very low intensity. This work has permitted to put into evidence the effect of the gamma ray of the $^{103}$Pd on the microdosimetric parameters. As these photons are attenuated much more slowly than the 20 keV photons in water, there is a hardening of the radiation with the distance for $^{103}$Pd that does not exist for $^{125}$I. This hardening induces a slight shift of the MS toward the smaller value of *y* and a small decrease of $\bar{y}_D$ with distance.

Some calculations have been performed too for model 6711 from Amersham showing the influence of the fluorescence X-rays of 22 keV produced in the silver core of that seed. The presence of those rays decreases the mean energy of the photons emitted by these sources and potentially enhanced their biological effectiveness.

## 2. The ionization cluster approach

The use of the microdosimetry concepts is one kind of approach. Another kind of studies has been performed to analyse the energy deposition on smaller scales in the form of cluster analysis. This information in very small region is indeed very relevant as the range of the secondary electrons is extremely short. Monte Carlo techniques allow calculations to be performed down to nanometre distances, in which region direct experimental data are difficult to obtain and analytical methods based on LET and cord length distribution are not applicable. However, the information contained in these tracks must be summarised and simplified. One possible way of doing so is to use the cluster concept (Michalik 1991, Michalik 1993).

In that approach, the conventional cluster algorithms designed for analysis of more dimensional data is applied to the track structure classification. In this study, the tracks are calculated with TRION and analysed segment by segment. A home-written program, CLUSTAN (Verhaegen 1996) is used to find clusters of ionizations formed by *j* ionizations contained in a sphere of radius *p* around a virtual centre. If the cluster contains j ionizations, it is said to be a cluster of order j. The distribution *h(j, p)* is computed. The form of the distributions depends on the ratio of the parameter *p* to the mean free path between ionizations, $l_i$. *For*

$p/l_i << 1$, the cluster of order 1 will be the most probable and the probability of occurrence of high-order clusters will decrease rapidly. With increasing ratio $p/l_i$, the spectra will be wider and the greater the $p/l_i$ the more probable will be the occurrence of the higher order clusters.

a) Results (see p 145)

The primary electron spectra have been calculated using the EGSnrc code. We have used the flexibility of this code that permits to select only the electrons generated in Compton or photoelectric events using the function IARG combined with the flag IAUSFL (Kawrakow 2003). These electrons have been tallied in bins according to their energy in order to obtain the primary electrons spectra that we needed. These spectra can be calculated at any position in the medium surrounding the seed. For each electron energy contained in these spectra, the cluster distribution is calculated. They are combined to obtain the cluster distribution for the complete primary electron spectrum.

INSTITUTE OF PHYSICS PUBLISHING PHYSICS IN MEDICINE AND BIOLOGY

Phys. Med. Biol. **49** (2004) 3781–3795 PII: S0031-9155(04)73651-9

# Theoretical analysis of microdosimetric spectra and cluster formation for $^{103}$Pd and $^{125}$I photon emitters*

**B Reniers**[1,3], **S Vynckier**[1] **and F Verhaegen**[2]

[1] Catholic University of Louvain, Cliniques Universitaires St Luc, 1200 Brussels, Belgium
[2] Medical Physics Unit, McGill University, Montreal, Quebec, Canada

Received 10 December 2003
Published 2 August 2004
Online at stacks.iop.org/PMB/49/3781
doi:10.1088/0031-9155/49/16/022

**Abstract**

In this work we have compared $^{125}$I or $^{103}$Pd from a microdosimetric point of view. The photon spectra at different positions around the seeds have first been calculated using EGSnrc Monte Carlo (MC) code. These photon spectra are used as input for the event-by-event MC code TRION to calculate the microdosimetric lineal energy ($y$) distribution for each isotope. The microdosimetric dose average lineal energy, $y_D$, calculated in a sphere of 1 $\mu$m is 3.5 keV $\mu$m$^{-1}$ for $^{125}$I and 4.0 keV $\mu$m$^{-1}$ for $^{103}$Pd, agreeing well with values reported in the literature. $y_D$ in a 1 $\mu$m sphere diminishes slightly with the distance from the seed for $^{103}$Pd. This is due to the spectral hardening caused by the presence of a gamma-ray of 357.5 keV in the initial spectrum of $^{103}$Pd. In parallel with the calculation of the microdosimetric spectra, we have analysed the distribution of the size of the energy deposition clusters generated by these low energy photons in structures of 2 and 10 nm of radius. Due to Compton interactions, the fraction of very low energy electrons ($<5$ keV) generated by $^{125}$I photons is 51%, whereas it is only 27% for $^{103}$Pd. As these electrons deposit their energy very locally, the pattern of energy depositions contains more clusters of a few nm of radius for $^{125}$I than for $^{103}$Pd; the mean cluster orders are respectively 3.3 and 3.0 for 10 nm clusters. This is in opposition with the prediction based on the microdosimetric spectrum and the parameter $y_D$ and could be of importance for the damage to the cells.

## 1. Introduction

Permanent implants of $^{125}$I or $^{103}$Pd are increasingly in use for the treatment of prostate tumours. They are also used for the treatment of other lesions such as eye tumours. This interest is primarily justified by the localization of their dose distribution due to the low energy

* Presented at the WC 2003, 03.05B: Second International Workshop on Mini and Micro Dosimetry and Its Applications.

[3] Present address: Service de Radiothérapie, Hôpital Maisonneuve-Rosemont, Quebec H1T 2M4, Canada.

0031-9155/04/163781+15$30.00  

photons emitted by these isotopes. Other advantages are the potential reduction in tumour repopulation due to the longer treatment time compared to external beam radiotherapy and the reduction of oxygen enhancement ratio with the decrease in dose rate that may partially circumvent the radioresistance of hypoxic cells (Ling 1992).

$^{125}$I has a mean photon energy of 28 keV. Due to the high attenuation of the low energy photons, this isotope provides a good sparing of the healthy tissues and a better radioprotection of the staff compared to other isotopes used in brachytherapy such as $^{192}$Ir. Its half-life of 59 days is however quite long; for a typical prostate implant, the initial dose rate at the prescription point is about 0.08 Gy h$^{-1}$. This dose rate could be too low for fast growing tumours. This is the reason why other isotopes, such as $^{103}$Pd, have been investigated. $^{103}$Pd has a mean photon energy of 20 keV, quite close to $^{125}$I but a shorter half-live of 17 days. For the same typical implant, the initial dose rate is 0.2 Gy h$^{-1}$. This initial dose rate is a parameter of importance, depending on the tumour doubling time, in the choice of the isotope. $^{103}$Pd seems more efficient for fast growing tumours while $^{125}$I could be more adequate for slow growing tumours (Ling 1992).

Another important parameter regarding the choice of the isotope can be their relative biological effectiveness (RBE) compared to a $^{60}$Co beam. This RBE depends on the spatial pattern of energy distribution. There have been only a few studies on the RBE of $^{125}$I and $^{103}$Pd based on radiobiological or microdosimetric considerations (Wuu *et al* 1996, Wuu and Zaider 1998). The results reported for $^{125}$I vary between 1.2 and 2 for dose rates between 0.03 and 9 Gy h$^{-1}$ (Scalliet and Wambersie 1987). The values reported for $^{103}$Pd in the radiobiological study of Ling *et al* (1995) is 1.9 $\pm$ 0.7. Two other microdosimetric studies (Wuu *et al* 1996, Wuu and Zaider 1998) show results of 2.2 and 1.6.

In the present study, we have calculated microdosimetric distributions of the lineal energy $y$ for $^{103}$Pd and $^{125}$I using the event-by-event MC code TRION (Lappa *et al* 1993). According to the theory of dual radiation action of Kellerer and Rossi (1972) for low dose rate and/or low dose, the RBE can be related to these distributions using the dose-mean of the lineal energy distribution, $y_D$. We have investigated the variations of the microdosimetric parameters, $y_D$ and the microdosimetric spectra, with the distance from the source. This is relevant because most of the organs at risk that must be protected are quite distant from the sources.

However, in the generalized formulation of the theory of dual radiation action (Kellerer and Rossi 1978), this approach has been shown to have limitations, especially for radiations whose ranges are shorter than the chosen diameter of the sphere. So, as TRION is able to generate complete radiation tracks, these tracks have been used to locate the clusters of ionizations, which are very relevant from a radiobiological point of view. In fact, the formation of DNA double strand breaks supposedly requires two or more spatially correlated ionizations. So the molecular damages of DNA are closely related to the very local concentration of energy deposition in particle tracks (Michalik 1991, Goodhead and Brenner 1983, Goodhead and Charlton 1985, Goodhead 1987). A description of track structure, reflecting spatial distribution of ionizations, could allow an estimation of the yield of the different molecular damages of DNA.

The photon energies of $^{125}$I and $^{103}$Pd are situated in a region where the relative importances of Compton scattering and photoelectric absorption are competing. Due to Compton interaction, the fraction of very low energy electrons ($<$5 keV) generated by $^{125}$I photons is 51% whereas it is only 27% for $^{103}$Pd. As these electrons deposit their energy very locally, the pattern of energy depositions of $^{125}$I could contain more clusters of a few nm of radius than for $^{103}$Pd. This could be of importance for the damage to the cells. So, in the second part of this work, we have investigated the formation of clusters for the two mentioned isotopes using an in-house code called CLUSTAN (Verhaegen 1996).

## 2. Materials and methods

In this work, we have obtained information about the behaviour of low energy photons from $^{103}$Pd and $^{125}$I in microscopic or nanometric regions. The event-by-event MC code TRION (Lappa *et al* 1993) is used to calculate the microdosimetric spectra around these sources; the input data for these calculations are the photon spectra around the source at the positions of interest calculated using the MC code EGSnrc (Kawrakow and Rogers 2003). For the calculation of cluster distributions in nanometric regions, the input data are the primary electron spectra at the positions of interest.

### *2.1. Theoretical background: microdosimetric parameters*

The goal of microdosimetry is to evaluate the radiation effect in a small volume of matter, i.e. a volume of a size of biological interest, such as the volume of a DNA helix (radius of 2 nm), nucleosome (typical radius of ±25 nm), chromosome (about 1 $\mu$m), cell nucleus (a few $\mu$m) or a biological cell (about 10 $\mu$m). In such small volumes, the concept of absorbed dose fails, as the amount of absorbed energy during an event is highly variable. Some other fundamental quantities must then be used (ICRU 1983). The elementary quantity in microdosimetry is the *energy deposit*, $\varepsilon_i$ (J or eV). It is the energy deposited in a single interaction, $i$, defined as

$$\varepsilon_i = T_{\text{in}} - T_{\text{out}} + Q_{\Delta m}$$

where $T_{\text{in}}$ is the energy of the incident ionizing particle (exclusive the rest mass), $T_{\text{out}}$ is the sum of the energies of all ionizing particles leaving the interaction (exclusive the rest mass) and $Q_{\Delta m}$ is the change of rest mass energy of the atom and all the particles involved in the interaction ($Q_{\Delta m} > 0$: decrease of rest mass; $Q_{\Delta m} < 0$: increase of rest mass).

The *energy imparted* to the matter in a volume, $\varepsilon$, is the summation of all the energy deposits in that volume. The energy deposits over which the summation is performed may be due to one or more energy deposition events. The ratio of the energy imparted to the mass of the volume considered, $\varepsilon/m$, is the *specific energy*, $z$, expressed in Gy. In this study, we used the *lineal energy*, $y$ (keV $\mu$m$^{-1}$). It is the ratio, $\varepsilon/l$, of the energy imparted to the matter in a given volume by a single energy deposition event, and $l$, the mean cord length of that volume that results from the random interception of the site by a straight line.

These three quantities are stochastic quantities, which can be expressed by probability distributions. The probability density $f$ of the variable $y$ is the *lineal energy distribution* $f(y) = \frac{\mathrm{d}F(y)}{\mathrm{d}y}$ where the cumulative distribution function $F(y)$ is the probability that the lineal energy due to a single event is equal or less than $y$. The expectation value of this variable, $\bar{y}_F = \int_0^\infty yf(y)\,\mathrm{d}y$, is called the *frequency mean lineal energy*. This is a non-stochastic quantity. It is also of interest to consider the fraction of the absorbed dose delivered with a lineal energy less or equal to $y$, $D(y)$. The dose probability density, $d(y)$, is the derivative of this function with respect to $y$: $d(y) = \frac{\mathrm{d}D(y)}{\mathrm{d}y}$. The expectation value of this function is called *dose-mean lineal energy*: $\bar{y}_D = \int_0^\infty yd(y)\,\mathrm{d}y$. What is usually called a *microdosimetric spectrum* is the dose probability density multiplied by $y$: $yd(y)$.

One of the remaining concerns is the choice of the relevant site size. In 1993, Wuu and Zaider (1993) have shown that spectra in a site of 1 $\mu$m of diameter seem to correlate very well with many biological effects. Sites of 1 $\mu$m are also recommended in ICRU (1983) and are very often used for measurements. Therefore, we have also used 1 $\mu$m sites in our analysis. However, as the size of the DNA, suspected to be the main target, is much smaller than 1$\mu$m, we have reduced the size of the target to 2 nm and 10 nm of radius for the analysis of the cluster formation.

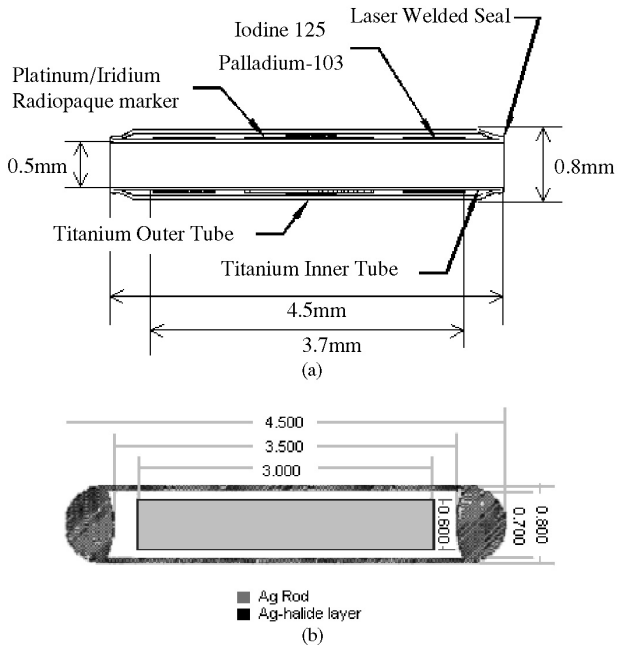


**Figure 1.** Schematic description of InterSource seed (IBt, Seneffe, Belgium) (a) and of Model 6711 seed (Amersham-Health) (b).

### *2.2. Description of the seeds*

The seeds we have used in this study are the $^{125}$I and $^{103}$Pd seeds from IBt, InterSource models, and Model 6711 from Amersham. Schematic geometries of these seeds are shown in figures 1(a) and (b). They have already been described elsewhere, together with their dosimetric characteristics (Meigooni *et al* 2000, 2002, Nath *et al* 1995, Reniers *et al* 2001, 2002). The InterSource model is composed of two concentric titanium tubes laser welded at the edges. The radioactive material is deposited on the inner tube in the form of three bands of painting. At the centre of this seed is a platinum–iridium x-ray marker. Model 6711 is composed of one titanium tube; the radioactive material is deposited on a silver core. This core is also used as an x-ray marker. Williamson (1991) has shown that the presence of the silver core in Model 6711 induces a reduction of the mean energy of this seed due to the production of the characteristic x-rays of 22 keV.

### *2.3. Calculations*

*2.3.1. Photon and electron spectral calculations.* The complete photon spectrum for the three seeds has been calculated in water using the EGSnrc (Kawrakow 2000, Kawrakow and Rogers 2003) usercode FLURZ for distances from the seed ranging from 0.1 cm to 7 cm. The scoring regions were cylindrical shells of 1 mm length and 1 mm thickness, situated on the seed transverse axis and centred with respect to the seed longitudinal axis. The widths of the energy bins of the photon spectra used to calculate the microdosimetric spectra were 1 keV up to 40 keV, 10 keV up to 50 keV, 50 keV up to 100 keV and 100 keV up to 500 keV. We

**Table 1.** Initial photon spectra used in the EGSnrc MC simulation.

| $^{125}$I | | $^{103}$Pd | |
|---|---|---|---|
| Energy (keV) | Relative intensity | Energy (keV) | Relative intensity |
| 3.77 | 0.1500 | 20.1 | 0.2206 |
| 27.20 | 0.3980 | 20.2 | 0.4193 |
| 27.47 | 0.7420 | 22.7 | 0.1305 |
| 31.00 | 0.2580 | 39.8 | 0.0007 |
| 35.46 | 0.0667 | 357.5 | 0.0002 |

have included in FLURZ the complete geometry of the seed, except for the conical shape of the edges, which has been approximated by cylinders. We have checked that it has a negligible influence on the transverse axis. In FLURZ, the photons were transported down to 1 keV; the electrons were not transported (cut-off of 1.5 MeV); the bound Compton scattering, Rayleigh scattering and atomic relaxations cross sections were used. Five hundred million 'histories' were necessary to achieve a statistical uncertainty of 1.1% on the mean energy at 7 cm. The initial spectra for $^{125}$I and $^{103}$Pd used in the simulations, taken from the NuDat program (Kinsey *et al* 1997)[4], are reported in table 1. In contrast to other studies, we have decided not to neglect the photons of 357.5 keV in the palladium spectrum, even though its relative intensity is extremely low.

As we needed more flexibility to calculate the primary electron spectra generated by the photons in water around the source, an in-house EGSnrc usercode is used instead of FLURZ. The same geometry is used to model the seed. Photons are transported down to 1 keV. The energies of the electrons created after Compton interactions or photoelectric effects in the desired regions, selected using the IARG flag capability of EGSnrc, are stored, down to 100 eV, as an energy spectrum.

*2.3.2. Microdosimetric simulations.* To calculate the microdosimetric parameters for $^{125}$I and $^{103}$Pd, we have used the event-by-event Monte Carlo code TRION (Lappa *et al* 1993). This code is able to simulate transport and calculate microdosimetric and radiobiological characteristics for electrons, photons and ions ($Z \leqslant 10$) in a tissue equivalent material i.e. water vapour with unit density. In the process of particle transport through matter, the ionizations of outer shell as well as inner shell, excitations and elastic scattering of electrons are individually simulated by sampling with their representative cross sections. The set of cross sections used has been carefully tested by comparison with the available theoretical and experimental data (Lappa *et al* 1993). During the transport, the energy cut-off was set to 13 eV, as it is the energy needed to ionize a water molecule. 150,000 particles were used for each photon energy.

In TRION, the calculations of the microdosimetric quantities are based on the electron slowing down spectra. The microdosimetric spectra (MS) have been calculated for monoenergetic photons ranging from 4 to 400 keV with the same resolution in energy as the photon spectra. The two sets of spectra have then been folded to obtain the MS for the polyenergetic radiations.

*2.3.3. Cluster calculation.* TRION generates track structure files containing the positions and the type (soft or hard ionization and excitation) of each interaction along the trajectory of the electrons created during a single collision of the initial photon. In fact, the code

[4] Updated to http://www-nds.iaea.org/nudat2 on 2 June 2004.

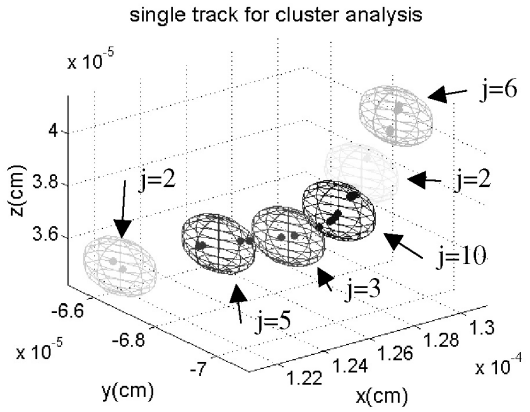


**Figure 2.** Example of CLUSTAN results. The dots are the positions of the ionizations along a part of an electron track. Spheres have a radius of 10 nm and contain the clusters found along a sample of 30 ionizations of the track of an electron of 10 keV. Six clusters were found with order $j$ from 2 to 10. Two ionizations remained solitary.

transports only electrons down to their energy cut-off of 13 eV, for photons, it treats only the first interaction and then follows the secondary electrons. The first step is to select only the ionizations, as they are responsible for the DNA breaks. Then an in-house developed program called CLUSTAN (Verhaegen 1996) permits to analyse the spatial distribution of these ionizations. This program searches in the list of ionizations those grouped in spherical clusters of a given radius, $p$. If the cluster contains $j$ ionizations, it is said to be a cluster of order $j$ (Michalik 1991). The program determines the distribution $h(j, p)$. When this distribution is computed for a sufficiently high number of tracks, it reflects the ability of a given radiation to form ionization clusters (see figure 2).

Due to calculation time considerations, it was not possible to analyse the full trajectory of the particles except for very low energy electrons, typically below 1 keV, where each track contains on average less than 35 ionizations. For higher energies, each electron track was divided into segments of 30 ionizations and only approximately 1/3 of these segments were analysed to find the clusters they contained. In order to calculate the distribution for the full track, the number of clusters found in each sample was added and weighted according to the fraction of the ionizations that have been analysed. The advantage of this method is that samples are collected in the beginning as well as in the end of the track. This is of importance as the energy of the particles is decreasing from the beginning to the end of the trajectory and consequently, the expected number of clusters of high order is increasing at the end of the track.

For the cluster analysis, we use the primary electron spectrum set in motion in water by the photons emitted by the seeds. TRION can calculate tracks only for monoenergetic primary electrons. To take into account the polyenergetic characteristic of the radiation of the seeds, the spectra are folded afterwards according to the frequency spectrum of the primary electrons in the same way as described for the microdosimetric spectra. In this case, we emphasize the effects of low energy photons and have consequently neglected the high energy component of the radiation, above 40 keV. Consequently, it is not possible to investigate the effect of the distance as this effect is due to the hardening of the radiation caused by the presence of the 357.5 keV gamma-ray.

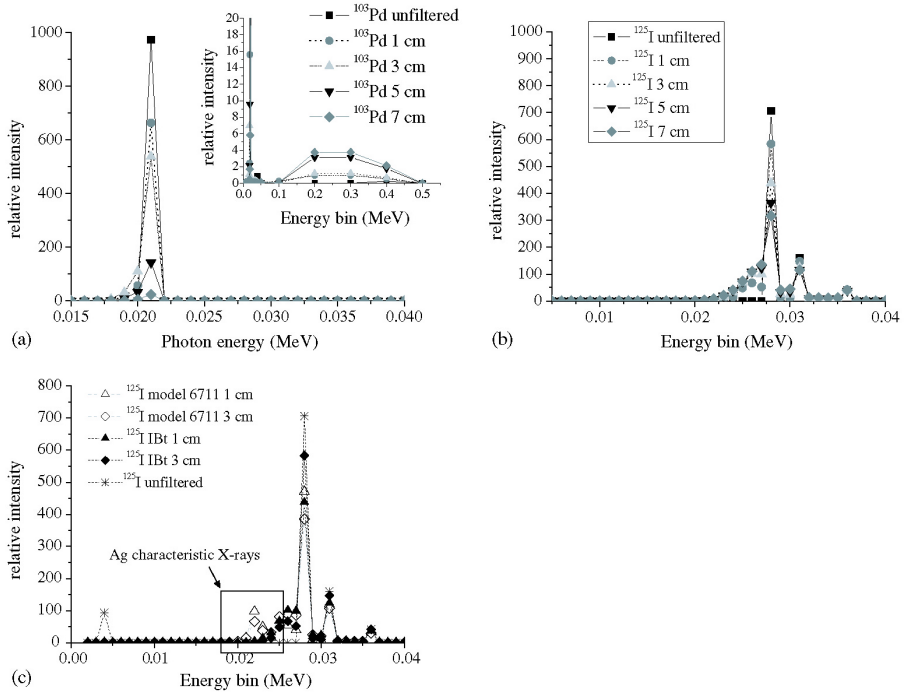


**Figure 3.** Calculated photon spectrum for InterSource$^{103}$ palladium seed in water for depths between 1 cm and 7 cm, and the unfiltered spectrum. The insert shows the complete photon spectrum up to 500 keV (a). Same for InterSource$^{125}$ iodine seed (b) and comparison of the spectrum of model InterSource$^{125}$ and Model 6711 for depths of 1 and 3 cm in water (c).

## 3. Results

### *3.1. Photon spectra*

Before calculating the microdosimetry spectra, we generated the initial photon spectra at several points of interest around the seeds. Some of the results are presented in figures 3(a)–(c). The spectra were normalized to unity area. They were calculated in water at different distances from the source (0.1, 0.2, 0.3, 0.4, 0.5, 1, 2, 3, 4, 5, 6, 7 cm). For the $^{125}$I seeds, the initial spectrum is composed of five photon rays, from which the lowest energy is 3.77 keV. The encapsulation material immediately absorbs these extremely low energy photons; therefore they do not contribute to the spectral and dose distribution around the seed (figures 3(b) and (c)). The spectrum varies only slightly with the distance; only scattered photons appear. Figure 3(c) shows the presence of the characteristic x-rays of silver in Model 6711.

For palladium, the situation is slightly different. The initial spectrum is mainly composed of three x-rays with close energies: 20.1, 20.2 and 22.7 keV, and one ray at 39.7 keV; but $^{103}$Pd also emits gamma-rays; the most important, of a very low intensity however, is at 357.5 keV. The attenuation with distance of the 20 keV photons is much faster than the attenuation of the 357 keV photons, so there is a hardening of the radiation spectrum with the distance for the palladium seed. The contribution of the gamma-ray at large distance from the source is not negligible even if its initial intensity is so weak that usually it is not considered. The mean

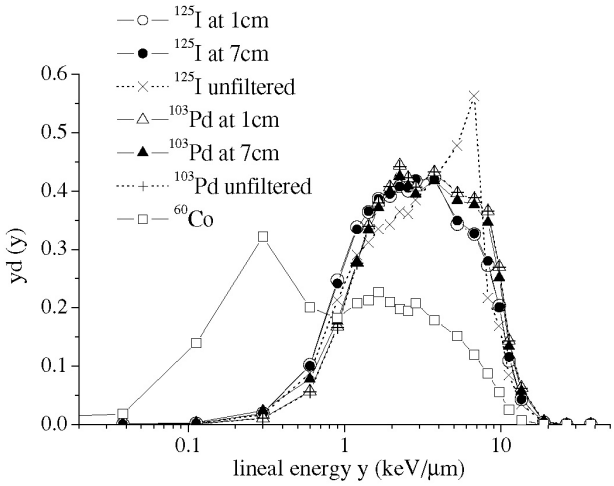


**Figure 4.** Microdosimetric spectra in 1 $\mu$m sphere for $^{125}$I and $^{103}$Pd at two distances from the source and unfiltered and for a simplified spectrum of $^{60}$Co.

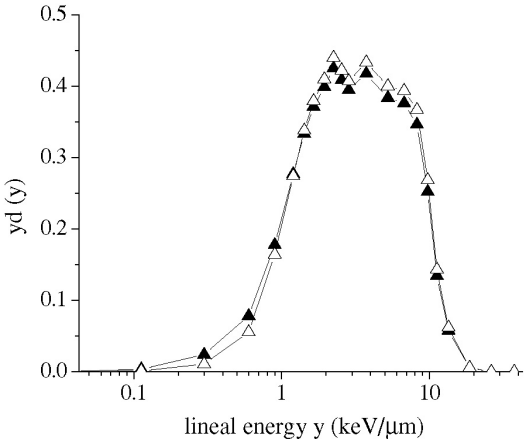


**Figure 5.** Effect of hardening due to the presence of the gamma-ray of 357.5 keV for the palladium seed on the microdosimetric spectrum at 7 cm. Open symbols are the MS calculated using a photon spectrum neglecting the gamma-ray; full symbols are the MS taking into account these high energy photons.

energy is modified from 20.6 keV at 0.2 cm from the source to 26.5 keV at 7 cm from the source, which represents a mean energy very close to the $^{125}$I mean energy.

### *3.2. Microdosimetry spectra*

The calculated MS are presented by figures 4–6. Figure 4 compares the MS calculated in a site of a diameter of 1 $\mu$m for InterSource$^{125}$ and InterSource$^{103}$ in water between 1 cm and 7 cm

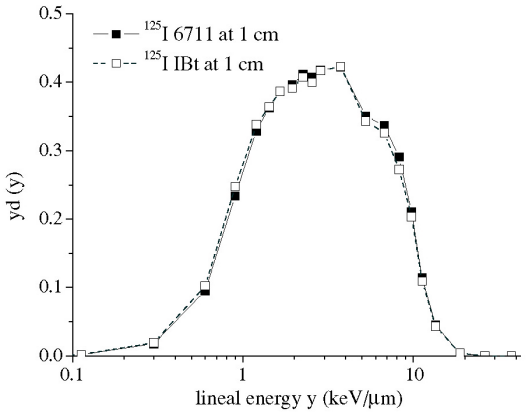


**Figure 6.** Comparison of the microdosimetric spectra for $^{125}$InterSource and Model 6711.

Only a few relevant distances are displayed. They are compared to the MS calculated with the same method for $^{60}$Co. For this isotope, the MS has been calculated using a simplified photon spectrum with the two main lines of 1173 and 1332 keV only. This figure shows that the low energy photons of the $^{103}$Pd and $^{125}$I photons induce, as expected, a shift in the MS spectra to the higher values of lineal energy compared to higher energy photons as emitted by $^{60}$Co. There is a small but visible effect in these MS due to the hardening of the $^{103}$Pd photons with the distance from the source. It induces a small shift of the MS towards the smaller value of the lineal energy. As shown in figure 5, this shift of the $^{103}$Pd spectrum for large distances is due to the presence of the high energy gamma-ray in the initial spectrum. Indeed, this effect disappears when the MS calculations ignore this gamma-ray. For $^{125}$I, the MS are identical at any distance. For this isotope, figure 6 compares the MS of InterSource$^{125}$ and Model 6711. The presence of the Ag characteristic x-rays of 22 keV in Model 6711 has also an effect on the MS, even if it is extremely small. It induces a small shift towards the higher lineal energy as the mean energy of the radiation decreases.

In figure 4, the MS for the initial spectra of $^{103}$Pd and $^{125}$I without filtration is also shown. The presence of the very low energy photons at 3.77 keV in the spectrum of $^{125}$I explains the presence of the peak at 6.5 keV $\mu$m$^{-1}$. These very low energy photons are in practice filtrated by the encapsulation of the seed. This peak could only be of importance in the case of a contamination with $^{125}$I. In this case, the 3.77 keV photons could increase the biological effect of this isotope for very short distances.

From these MS, one can calculate the parameter $y_D$ related to the RBE in the theory of dual radiation action (Kellerer and Rossi 1972). Figure 7 displays the value of this parameter at different distances for the three types of seeds in water. It shows that the variation of $y_D$ for the $^{103}$Pd seed starts only around 5 cm from the source; for smaller distances, the parameter is essentially constant. The ratio of $y_D$ for $^{103}$Pd and $^{125}$I is 1.14 at 0.1 cm. This ratio decreases to 1.09 at 7 cm from the source due to the decrease of $y_D$ for $^{103}$Pd with distance.

In table 2, the $y_D$ values are compared to the very few available experimental values (Wuu *et al* 1996). They have been measured using a grid-defined wall-less proportional counter equivalent to 1 $\mu$m at 1 cm depth in A-150 tissue equivalent plastic. Our calculations are in good agreement with these experimental data with 6.5% difference for $^{103}$Pd, 3% for $^{125}$I (Model 6711) and 1% for $^{60}$Co.

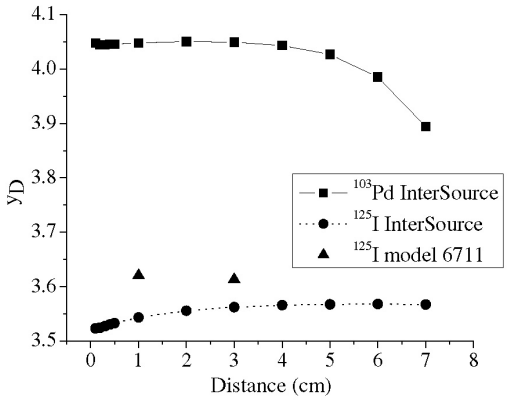


**Figure 7.** Variation of the parameter $y_D$ with the distance from the seed for InterSource$^{103}$, InterSource$^{125}$ and Model 6711.

**Table 2.** Comparison of the $y_D$ calculations of this study with the calculations and measurements published in the literature at 1 cm depth in water. The value in brackets is calculated from a photon spectrum calculated in A-150 at 1 cm depth.

| | Measured[a] (1 cm depth in A-150) | Calculated[a] | Calculated ratio to $^{60}$Co[a] | Measured ratio to $^{60}$Co[a] | Calculated (this work) | Calculated ratio to to $^{60}$Co (this work) |
|---|---|---|---|---|---|---|
| Pd-103 | 3.8 | 3.3 | 2.2 | 2.38 | 4.05 (4.05) | 2.57 |
| I-125 (6711) | 3.5 | 3.0 | 2.0 | 2.19 | 3.61 | 2.28 |
| I-125 (IBt) | | | | | 3.54 | 2.24 |
| Co-60 | 1.6 | 1.5 | 1.0 | 1.00 | 1.58 | 1.00 |

[a] Wuu *et al* (1996).

### *3.3. Cluster analysis*

The input data for the cluster calculations are the primary electron spectra. They are shown in figure 8 for $^{125}$I and $^{103}$Pd at 0.5 cm from the source. For the cluster analysis, we have reduced the dimension of the targets from 1 $\mu$m to 2 nm and 10 nm, as this size is more representative for the DNA molecules. Figures 9(a) and (b) show some examples of cluster distributions calculated for monoenergetic electrons between 100 eV and 35 keV, for the cluster distribution of 2 nm radius and 10 nm radius, respectively. In figure 9(b), electrons of 300 keV, representative for $^{192}$Ir sources, are also presented for comparison. As expected, the frequency of single ionizations is decreasing when the energy of the electrons decreases, or, in other words, the ionization cluster order is increasing with decreasing energy. For the very low electron energy however, this is compensated by the fact that the number of ionizations per track decreases. Figure 10 gives the mean cluster order in function of the electron energy. It shows the existence of a maximum in the mean cluster order for electrons of about 300 eV when considering clusters of 2 nm radius and of about 500 eV for clusters of 10 nm radius. The insert graph shows the fraction of ionizations grouped into mean order clusters. It shows that for 100 eV electrons, close to 100% of the ionizations are included in a 2 nm cluster of the mean order, 2.8, and for clusters of 10 nm, all the ionizations are included in clusters of the mean order up to 300 eV. So, it can be deduced that below these energies, 100 eV for 2 nm and 300 eV for 10 nm, electron tracks contain, on average, only one cluster. In that case, when

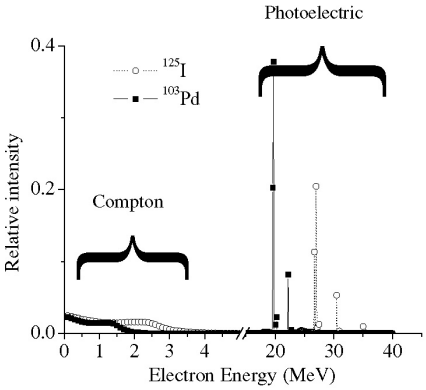


**Figure 8.** Primary electrons spectra of $^{125}$I (dotted line) or $^{103}$Pd (full line).

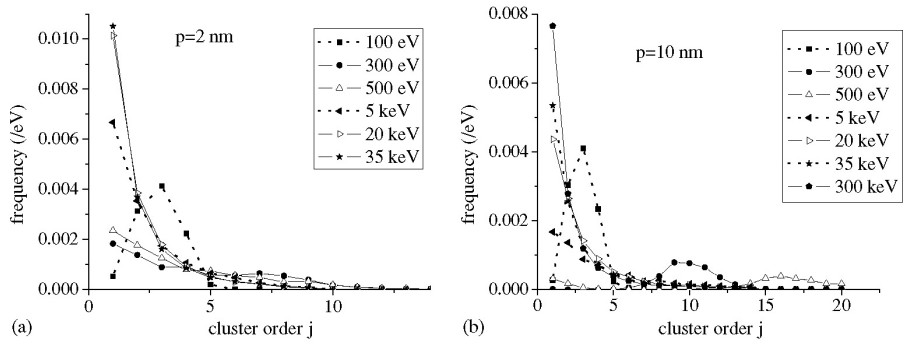


**Figure 9.** Some examples of cluster distribution for monoenergetic electrons in a site of 2 nm (a) and in a site of 10 nm (b).

the number of ionizations per track decreases, so is the mean cluster order. This explains too why the cluster distributions for electrons of 100 eV are the same for clusters of 2 nm and 10 nm. It means only that for these very low energies, all the ionizations are grouped in a region even smaller than 2 nm, so the distribution of the number of clusters becomes the distribution of the number of ionizations per track.

This information for monoenergetic electrons has been folded to calculate the cluster distributions for the isotopes. Figure 11 shows these distributions calculated for $^{125}$I and $^{103}$Pd spectra for 10 nm and 2 nm. The distributions calculated for $^{125}$I and $^{103}$Pd are very close to each other. However, it is interesting to note that, in contrast to the results for $y_D$ in a 1 $\mu$m sphere, $^{125}$I seems to induce less single ionizations than $^{103}$Pd. The mean order for clusters of 2 nm for $^{103}$Pd is 2.2 whereas it is 2.3 for $^{125}$I. For clusters of 10 nm, the mean cluster order is 3.0 for $^{103}$Pd and 3.3 for $^{125}$I. For comparison, the mean order of cluster of 10 nm created by electrons of 300 keV, as with $^{192}$Ir, is 2.1. It climbs to 8.8 for electrons of 1 keV.

## 4. Discussion

In this work, we have applied two methods to determine theoretically the biological effectiveness of the low energy photons emitted by $^{103}$Pd and $^{125}$I compared to photons of

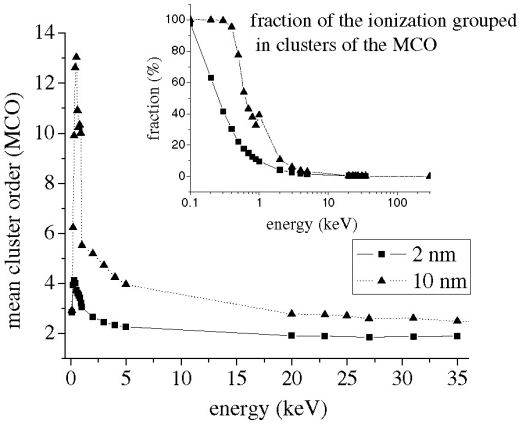


**Figure 10.** Mean cluster order in function of the electron energy for clusters of 2 nm and 10 nm. The insert shows the fraction of the ionizations produced in the electron tracks that are grouped in those mean order clusters.

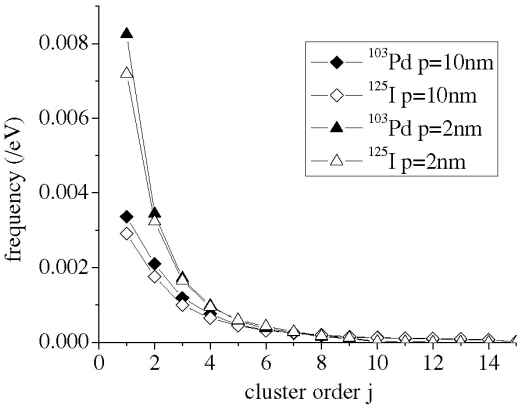


**Figure 11.** Distributions of the number of clusters of order between 1 and 14 of a radius of 10 nm and 2 nm for $^{125}$I and $^{103}$Pd per eV deposited energy.

higher energy such as $^{60}$Co or $^{192}$Ir. The first technique is the calculation of the microdosimetric spectra in a 1$\mu$m diameter sphere. To validate our calculations for a 1 $\mu$m target, we have used the measured MS published in the literature (Wuu *et al* 1996). We observe a good agreement with the measurement data. The MS calculated for $^{103}$Pd are slightly shifted towards the higher lineal energy values compared to $^{125}$I. The influence of silver x-rays produced in $^{125}$I seeds containing a silver core, like Model 6711, can be seen on the MS and on the $y_D$ value. It shows that the internal composition of the seeds has not only an influence on the dosimetric data but also on the microdosimetric data around the source, as it has already been pointed out by Taschereau *et al* (2002).

The effect of the high energy gamma-rays emitted by $^{103}$Pd has also been put in evidence. These photons induce a hardening of the radiation spectrum at larger distances. Consequently,

the mean energy of the photons of $^{103}$Pd at 7 cm of 26.5 keV is not very different from the mean energy of $^{125}$I. The effect on the MS is not as drastic because the spectrum is still very different from the $^{125}$I spectrum, but it induces a small shift of the MS of $^{103}$Pd towards lower $y$ values. This is of course a very small effect compared to the much more biologically important effect of the decrease of the dose rate with the distance. However, this is an additional factor to take into account for $^{103}$Pd.

For these calculations, we have adopted the classical microdosimetric sphere of 1 $\mu$m diameter (ICRU 1983), but several authors have pointed out that the main target to assess biological damage is DNA. As the cross-sectional diameter of DNA is a few nanometres, we have reduced the size of the site to 2 nm and 10 nm in these calculations. For these extremely small volumes, the determinant parameter is the distribution of the individual energy deposition events inside the DNA. So, for this second part, we have used a second approach consisting of the analysis of the distribution of the ionization clusters produced by the electrons generated by the photons during a single collision in the matter.

The conclusion of this analysis is that in such very small volumes, $^{125}$I produces slightly more high-order clusters than $^{103}$Pd. It is due to the fact that Compton interaction is still predominant for $^{125}$I, while its importance is small compared to photoelectric effect for $^{103}$Pd. For $^{125}$I, 51% of the interactions are Compton type, while they are only 27% for $^{103}$Pd. During Compton interaction, electrons of very low energy are created. The maximum energy for these electrons for the $^{125}$I photon energy is 4.3 keV. These electrons deposit their energy very locally. Their range in water is at most 530 nm. Consequently, those electrons produce many ionizations in very small volumes and are then very efficient for DNA damage. Those particles are exactly the cases where the theory of dual radiation action finds one of its limitations as their range is smaller than the site where the MS are calculated.

In relation to this cluster analysis, it must be reminded however that TRION uses cross sections for vapour water and not for liquid water. As the energy needed to create an electron–ion pair, the $W$-value, is higher for vapour than for liquid for these electron energies, the number of ionizations is underestimated by a factor between 1.5 and 1.2 with our method (Paretzke *et al* 1986, 1991). In addition, the calculation in vapour does not take into account the collective effects that exist in the condensed phase (plasmons) and that can delocalize the effect of the energy loss. However, it must be clear that this work intends to address only partially the problem of interaction of radiation with living cells. The real problem does not only depend on the ionization pattern in water but is rather a complex problem involving interactions between radiation and DNA molecules, very different from water, and with the water molecules around the DNA, which cannot be considered as vapour or liquid, but rather as crystalline water. Nevertheless, the quite simple approach we use here can bring some basic information concerning ionization patterns in a very simple and very well-known medium. Moreover, the relative information we deduce from our calculations and the importance of low energy electrons should still be relevant for liquid water.

In conclusion, the microdosimetric and nanodosimetric data obtained from our calculations are quite close for $^{103}$Pd and $^{125}$I. A few effects have, however, been pointed out like the effect of the distance from the seed for $^{103}$Pd or the effect of the silver characteristic x-rays for $^{125}$I seeds. Moreover, the cluster study has shown that the very low energy electrons created during Compton interactions could have a significant influence on the type of damages induced in DNA as they produce high-order ionization clusters.

The inversion of the relative effectiveness of $^{103}$Pd compared to $^{125}$I between the results obtained in micrometric size sites and nanometric size sites shows once more how important is the determination of the real target size for relevant biological systems. Physics can bring some important information, but at this stage, it is only with more biological data that we

will be able to improve further our knowledge of the fundamental mechanisms involved in the interaction between radiation and living tissues.

## Acknowledgments

This work was supported by a grant from the Belgian 'Fonds National pour la Recherche Scientifique' (F.N.R.S.). Travel support from IOP enabling the presentation of this work at the WC2003 Conference on Biomedical Engineering is also gratefully acknowledged.

## References

Goodhead D T and Brenner D J 1983 Estimation of a single property of low LET radiations which correlates with biological effectiveness *Phys. Med. Biol.* **28** 485–92

Goodhead D T and Charlton D E 1985 Analysis of high-LET radiation effects in terms of local energy deposition *Radiat. Prot. Dosim.* **13** 253–8

Goodhead D T 1987 *Physical Basis for Biological Effect Nuclear and Atomic Data for Radiotherapy and Related Radiobiology* (Vienna: IAEA) pp 37–53 (ISBN 92-0-131087-0)

ICRU 1983 *Microdosimetry ICRU Report 36* (Bethesda, MD: International Commission of Radiation Units and Measurements (ICRU))

Kawrakow I 2000 Accurate condensed history Monte Carlo simulation of electron transport: I. EGSnrc, the new EGS4 version *Med. Phys.* **27** 485–98

Kawrakow I and Rogers D W O 2003 The EGSnrc code system: Monte Carlo simulation of electron and photon transport *Report PIRS-701* Ottawa, National Research Council of Canada (NRCC) (http://www.irs.inms.nrc.ca/inms/irs/EGSnrc)

Kellerer A M and Rossi H H 1972 The theory of dual radiation action *Curr. Top. Radiat. Res. Q.* **8** 85–158

Kellerer A M and Rossi H H 1978 A generalized formulation of dual radiation action *Radiat. Res.* **75** 471–88

Kinsey R R, Dunford C L, Tuli J K and Burrows T W 1997 The NUDAT/PCNUDAT Program for Nuclear Data, *Proc. 9th Int. Symposium on Capture Gamma-Ray Spectroscopy and Related Topics (Budapest, Hungary, October 1996)* p 657 (http://www-nds.iaea.or.at/nudat/)

Lappa A V, Bigildeev E A, Vasilev O N and Burmistrov D S 1993 TRION Code for radiation action calculation of and its applications in microdosimetry and radiobiology *Radiat. Environ. Biophys.* **32** 1–19

Ling C C 1992 Permanent implants using Au-198, Pd-103 and I-125: radiobiological considerations based on the linear quadratic model *Int. J. Radiat. Oncol. Biol. Phys.* **23** 81–7

Ling C C, Li W X and Anderson L L 1995 The relative biological effectiveness of I-125 and Pd-103 *Int. J. Radiat. Oncol. Biol. Phys.* **32** 373–8

Meigooni A S, Sowards K and Soldano M 2000 Dosimetric characteristics of the InterSource $^{103}$palladium brachytherapy source *Med. Phys.* **27** 1093–100

Meigooni A S, Yoe-Sein M M, Al -Otoom A Y and Sowards K T 2002 Determination of the dosimetric characteristics of InterSource$^{125}$ iodine brachytherapy source *Appl. Radiat. Isot.* **56** 589–99

Michalik V 1991 Particle track structure and its correlation with radiobiological endpoint *Phys. Med. Biol.* **36** 1001–12

Nath R, Anderson L L, Luxton G, Weaver K A, Williamson J F and Meigooni A S 1995 Dosimetry of interstitial brachytherapy sources: recommendations of the AAPM Radiation Therapy Committee Task Group No. 43 *Med. Phys.* **22** 209–34

Paretzke H G, Turner J E, Hamm R N, Ritchie R H and Wright H A 1991 Spatial distributions of inelastic events produced by electrons in gaseous and liquid water *Radiat. Res.* **127** 121–9

Paretzke H G, Turner J E, Hamm R N, Wright H A and Ritchie R H 1986 Calculated yields and fluctuations for electron degradation in liquid water and water vapour *J. Chem. Phys.* **84** 3182–8

Reniers B, Vynckier S and Scalliet P 2001 Dosimetric study of the new Intersource$^{125}$ iodine seed *Med. Phys.* **28** 2285–8

Reniers B, Vynckier S and Scalliet P 2002 Dosimetric study of a new palladium seed *Appl. Radiat. Isot.* **57** 805–11

Scalliet P and Wambersie A 1987 Which RBE for iodine 125 in clinical applications? *Radiother. Oncol.* **9** 221–30

Taschereau R, Roy R and Pouliot J 2002 Relative biological effectiveness enhancement of a $^{125}$I brachytherapy seed with characteristic x rays from its constitutive materials *Med. Phys.* **29** 1397–402

Verhaegen F 1996 Biological dosimetry with radio-induced micronuclei in human lymphocytes: physical aspects and automatisation *PhD Thesis* University of Ghent, Belgium (in Dutch)

Williamson J F 1991 Comparison of measured and calculated dose rates in water near $^{125}$I and $^{192}$Ir seeds *Med. Phys.* **18** 776–86

Wuu C S, Kliauga P, Zaider M and Amols H I 1996 Microdosimetric evaluation of relative biological effectiveness for $^{103}$Pd, $^{125}$I, $^{241}$Am, and $^{192}$Ir brachytherapy sources *Int. J. Radiat. Oncol. Biol. Phys.* **36** 689–97

Wuu C S and Zaider M 1993 Microdosimetry of brachytherapy sources and specific quality function *Med. Phys.* **20** 879 (Abstract)

Wuu C S and Zaider M 1998 A calculation of the relative biological effectiveness of $^{125}$I and $^{103}$Pd brachytherapy sources using the concept of proximity function *Med. Phys.* **25** 2186–9

b) Complementary calculations

The distribution of clusters *h(j, p)* has been calculated for sites of 2 nm and 10 nm of radius for monoenergetic electrons and for electrons generated by the passage of the photons of $^{103}$Pd and $^{125}$I in water. From the MS in a micron sphere, it was expected that $^{125}$I would produce more clusters of high order than $^{103}$Pd, and consequently have less single interaction. But it is the opposite that has been obtained. $^{103}$Pd produces more single interactions than $^{125}$I. To support this, the microdosimetric spectra have been calculated in water for $^{125}$I and $^{103}$Pd as function of the distance for 4 different sizes of site, radius of 2 nm, 5 nm, 10 nm and 0.5 *m*m. Figure 47 shows the variation of the parameter $\bar{y}_D$ for these 4 sites sizes and in function of the distance. It is interesting to notice that the same inversion occurs for the parameter $y_D$ when the site size decreases. For the 0.5 µm radius site, $^{125}$I shows lower values of $\bar{y}_D$, when for 2 nm radii; $^{103}$Pd shows lower values of $\bar{y}_D$. The inversion seems to occur in the region of 5 nm to 10 nm of radius.

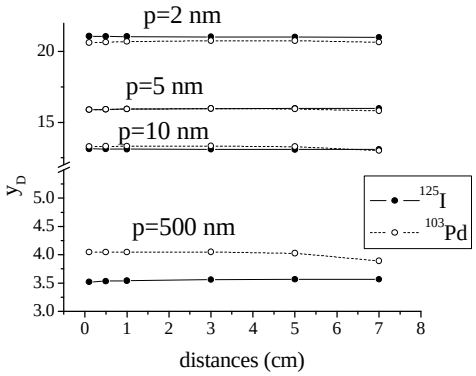


**Figure 47: Variation of the parameter $y_D$ as a function of the distance for different radii p of sphere.**

Contrary to the results we have obtained with the MS in 1 µm diameter sphere, $^{103}$Pd photons produce slightly more low order clusters than $^{125}$I, what means that it could have a slightly less, or at least equivalent, radiobiological effectiveness. As it is pointed out in the preceding paper, this shows the real need for biological data to assess the most relevant site size.

# V. Conclusion

This work is dedicated to the study of low energy photons emitted by $^{103}$Pd and $^{125}$I seeds used for brachytherapy applications like prostate or eye treatments. It includes different aspects: dosimetric and microdosimetric. The first part concerns the determination of the basic dosimetric parameters of two new types of such seeds. AAPM recommends that two studies based on measurements and/or on Monte Carlo calculations are performed in two independents laboratories for each new type of seed. The total of the two studies must contain calculations and measurements. In that context, we have determined for the first time the dosimetric data for the Iodine source "InterSource$^{125}$" from IBt and we have performed the second study for the palladium source "InterSource$^{103}$" from the same company. On the other hand, we have taken advantage of this basic study to analyse more closely some of the steps involved in this determination.

A general remark could be that the low energy photons differ in a fundamental way from the higher energy photons. Indeed, in megavoltage beams, or even already for $^{192}$Ir sources, Compton effect is dominant in water. In contrast, in the range of energies considered here, between 20 and 30 keV, photoelectric effect becomes of increasing importance. At 30 keV in water, about 40% of the interactions are of photoelectric type and at 20 keV, it climbs to about 65%. Moreover, as photoelectric effect is more or less proportional to $Z^4$, the effect of the presence of high Z components is enhanced. This invalidates many of the assumptions commonly made for the dosimetry in megavoltage beams. For example, the commonly used water substitutes, like polystyrene or polymethylmetacrylate (PMMA), or even specially engineered materials, like WT1 from RMI, cannot anymore be considered as water substitutes when used for low energy photons. If water equivalence is really needed, we have shown that new materials should be used, like for example, RW1 from PTW-Freiburg. It is even possible to question the use of water itself as tissue substitute at these energies as even soft tissues contain high-Z materials as Na, P, S, Cl or K in various amounts. These elements are traces only, but their cross sections for photoelectric effect are high, so their dosimetric importance must probably not be underestimated.

The great importance of photoelectric effect induces a high attenuation, which has a considerable influence on the measurements too. Firstly, the presence of the high gradients imposes the use of detectors with a high spatial resolution and a very precise positioning. TLDs are an ideal choice, also because of the generally low dose rates involved. We have however shown too that at these energies their presence, as small as they can be, should not be neglected. In contrast to the case of measurements in

megavoltage beams, they can not be considered as small cavities. Moreover, they induce a perturbation in the photon fluence whose consequence is that the TLDs can not be considered either as perfect large cavities,. The perturbation they introduce must be taken into account, especially for $^{103}$Pd. For absolute measurements, an additional concern arises from their energy correction factors. TLDs are usually calibrated in megavoltage beams or in $^{60}$Co ray beams; their response in those beams is very different from their response to $^{125}$I or $^{103}$Pd photons. Therefore, energy correction factors must be applied, which yields unfortunately supplementary uncertainties. The problem of the use of TLDs for low energies in itself is probably not trivial and would need some more investigations. For example, Monte Carlo calculations could be used to simulate their response at low energies and to compare it to megavoltage beams and thus calculate theoretically the energy correction factor. Some studies have been published on the subject but are still controversial (Das et al 1996, Davis et al. 2003). A few very preliminary simulations, not shown in this work, using point sources for $^{125}$I and $^{103}$Pd as well as for an imaginary 6MV linac beam seem promising.

In this study, we have used two different Monte Carlo codes, EGSnrc and MCNP4C. It was intended first as a consistency test only, but in the process, it has allowed us to investigate the basic databases used in these Monte Carlo codes. As these codes use different default cross section libraries, we have been able to show that the use of different cross section libraries can have an influence on the calculated clinical data, especially on the radial dose functions. For $^{125}$I, the deviations can be as high as 9% higher at 7cm from the seed with MCNP than with EGSnrc and it is even 17% at 5cm from a $^{103}$Pd seed. The main discrepancies between those databases concern the photoelectric effect cross sections; it has consequently an influence only for low energy photon sources. It was particularly serious for MCNP for which the default data for photoelectric effect differed from the XCOM distribution from the National Institute of Technology and Standard (NIST) by as much as 10% at 30 keV. For EGSnrc, the differences were smaller, but the data could still be improved. These databases were indeed improved, EGSnrc by Hobeila and Seuntjens (2003) from McGill University and MCNP4C by T. Bohm et al. (2003) from University of Wisconsin and thanks to the cooperation of these authors, we have been able to use updated libraries for both codes. That has reduced the differences between the results to the statistical uncertainties. Although the accuracy of the cross section database is still questionable, the comparison with experiments was also improved at the condition to use the perturbation correction factors for the TLD measurements. Indeed, very recently, AAPM has published an update to the TG-43 (Rivard et al. 2004) that recommends careful assessment of the type of cross section libraries used in the calculations. They recommend moreover being particularly meticulous regarding the correction factors to apply to the TLDs measurements.

Another question concerning the low energy photons concerns their biological effectiveness. The generally accepted hypothesis is that as the effectiveness of a radiation is related to the ionization density in matter, one should expect to see an effect when going from high energy photons to lower energies as the ionization density is increasing. However, there are only very few radiobiological data to support this hypothesis or, all the more so, to quantify it. It is not the goal of this work to study radiobiology, but some basic information can be gathered from purely physical mechanisms. The first possibility to try to obtain radiobiological information starting from purely physical data is to use the *theory of Dual Radiation Action* (Kellerer and Rossi 1972) or the generalised one (Kellerer and Rossi 1978). According to that theory, it is possible to deduce RBE from the microdosimetric $\bar{y}_D$ parameter in the case of low dose and/or low dose rate. In a first approach, it was the method we have used. We have not deduced RBE, but we have used $\bar{y}_D$ to compare the radiation quality. We have calculated the microdosimetry spectra in the classical volume used for this kind of studies, a sphere of 1 $\mu$m. Our results at 1cm from the seed in water are concordant with the results from the literature (Wuu et al. 1996). ). For $^{103}$Pd, $\bar{y}_D$ was found to be 4.05 keV/µm against 3.8 keV/µm in literature and for $^{125}$I $\bar{y}_D$ was found to be 3.6 keV/µm against 3.5 keV/µm in literature. We have shown however that for $^{103}$Pd, $\bar{y}_D$ varies with the distance from the seed due to the hardening of the photon spectrum of that isotope.

Moreover, the seeds themselves are made of different materials. Usually the encapsulation is in titanium, but they can contain other metals like silver, platinum or iridium. Although the dimensions of the seeds are extremely small, it was already shown that due the high attenuation of the photons, especially in metals, the interior design can influence in a noticeable way the dose distribution around the sources. It has been shown by several authors that even movements inside the seed could cause dosimetric modifications. But the position is not the only parameter, the type of metal is also important for the dosimetry, as for the effect of the X-ray fluorescence photons generated by silver. This justify once more, if necessary, the use of different dosimetric data for each type of seed. In the microdosimetric study, we have shown that the presence of those X-ray fluorescence photons has also a influence on $\bar{y}_D$, and consequently, on the potential radiobiological effectiveness as they lower the mean energy of the radiation.

In a second approach, we have used the following reasoning: It is acknowledged that the effectiveness of a radiation is related to the number of double stand breaks (DSB) produced in DNA molecules as these breaks, contrary to single strand breaks (SSB), can not be repaired. These breaks are caused by ionizations in or close to the DNA molecule. Thus using an event-

by-event Monte Carlo code called TRION (Lappa et al. 1993) and a home-made code called CLUSTAN (Verhaegen 1996), we have investigated the distribution of clusters of ionizations of 2 nm and 10 nm radii in water vapour with density 1. If a radiation produces a large number of clusters of high order (containing a large number of ionizations), it is more likely that if this radiation crosses a DNA molecule, it could cause DSB. From that assessment, it is then possible to compare radiations potential efficiencies by comparing their induced ionizations cluster distributions. So, we have compared $^{103}$Pd and $^{125}$I on that basis and found that in those extremely small volumes, the importance of the very low energy electrons created by Compton interactions should not be underestimated. Indeed, these electrons deposit their energy on extremely short distances; an electron of 1 keV has a range of 45 nm in water, much smaller than the ICRU sphere of 1 $\mu$m. As the energy of those electrons is very small, they have only a small effect on the microdosimetric spectra in 1µm spheres. The concentration of ionizations they produce however is very high and consequently very efficient to destroy DNA if those electrons are produced in the proximity of the molecule. The energies of $^{125}$I and $^{103}$Pd are very close, but it is the range of energies where the relative importance of Compton Effect and Photoelectric effect are switching in water, so interactions of $^{103}$Pd photons in water produce essentially photoelectrons when interactions of $^{125}$I in water still produce more Compton effects. $^{125}$I produce consequently more low energy electrons than $^{103}$Pd. When we compute the cluster distributions for these two isotopes, the effect of the low energy Compton electrons appears in the fact that $^{125}$I produces slightly more high order clusters than $^{103}$Pd, contrary to what was expected from the microdosimetric spectra analysis.

Of course, this is only a first step in the microdosimetric and nanodosimetric study, it would for example be very interesting to remove one of the most problematic approximations that has been done, from a physical point of view, namely, the fact that we analyse interaction in water, and not even in liquid water, but in water vapour. DNA is a very complex molecule, containing atoms of H, O, C, N, and P and even the first thin layer of water surrounding it is very special due to hydrogen bridges with the DNA molecule. As was shown extensively in this work, for photon interactions, the rapid increase of the photoelectric effect cross sections in the energy region we are considering implies that the real composition of the medium can not be approximated. On the other hand, when considering the transport of electrons down to a few eV, the state of the medium becomes important too due to the existence of collective effect in condensed matter.

Another still existing question that we have pointed out is the size of the target that we should use in this kind of study, i.e. classical microdosimetry or cluster analysis, as we found opposite results just by changing the scale of the analysis. This could only be solved however by more radiobiological studies. Some of these studies are currently in progress. One of these is an in-vivo study that concerns the regeneration of intestinal

crypts in mice after irradiation. That biological endpoint has been shown to be a good indicator of the biological effectiveness of the radiation (Withers and Elkind 1970). This technique has been used for many years by the research team of Dr Gueulette (Gueulette et al. 1996a, Gueulette et al. 1996b) for the study of biological effectiveness and the radiobiological calibration of non-conventional radiation beams. It has been used worldwide for the intercomparison of clinical beams of neutron, proton and heavy ion, and also for boron neutron capture therapy (BNCT) beams. That endpoint has recently been adapted to study the low energy photons of $^{125}$I and $^{103}$Pd (Ying et al. 2003). Some in-vivo measurements have been made recently with $^{125}$I compared to $^{60}$Co where the biological endpoint was the response of the treated tumour evaluated in terms of inhibition of growth (Lehnert et al. 2004). However the radiobiological studies for low energy isotopes are often facing the problem of the inhomogeneity of the dose rate. This interferes with the other parameters in the determination of radiobiological effect and could explain the large uncertainty still existing for the RBE of $^{125}$I and $^{103}$Pd.

In conclusion, low energy photons physics is a very interesting and a quite challenging domain in dosimetry. The use of low energy photons in brachytherapy will certainly continue to spread in the coming years and the developments in medical techniques and the increase of the know-how of the medical doctors will certainly induce the need for a more and more accurate dosimetry. Many studies have already reported the direct relation between dose to the prostate and PSA-free survival like for example Stock et al. (2002) or dose to the surroundings organs and urethra and morbidity like rectum bleeding (Zapatero et al. 2004, Merrick et al 2003), urinary disfunctions (Merrick et al. 2004, Salem et al. 2003) or erectile disfunctions (Merrick et al 2002). Discrepancies between Monte Carlo simulations are now explained by the cross section data, but uncertainties of 10% in the measured dosimetric data are still accepted in the last update of the TG-43 while for external radiotherapy, the precision on the absolute dose delivered for external radiotherapy should be less than 2%. It is evident that for brachytherapy it is not possible to avoid hot spots inside the tumour due to the presence of the sources, however, concerns about the eventual presence of cold spots can be raised as it has been shown to have a direct influence on the local relapse. On the other hand, even if the dose decreases very rapidly with the distance from the source, dose to organs at risk should be assessed with the maximum possible accuracy. For the level of doses used for eye treatments for example, a 10% difference on the dose delivered to the lens or to the optical nerve could perhaps be significant for the preservation of vision after the treatment. In the present state, it is however very difficult to assess as it is the limit of the precision on the dosimetric data.

So even if photons are considered as a very well-known radiation, detailed investigations should clearly be continued. As we have shown, improvement can be made regarding the dosimetry as for the different

correction factors that have to be used for TLD measurements. It would certainly be interesting also to investigate other detectors for the measurements. The developments in radiochromic film technology seems, for example, very promising and should be pursued. On the other hand, efforts are needed from radiobiologists to assess the Relative Biological Efficiency of these radiations. This, together with the development of event-by-event Monte Carlo codes, could help to understand the mechanism of interactions between radiations and living tissues at a very basic level and the interesting influence of the very low energy electrons that is, for the moment, only presumed. In the next few years, it is clear that cooperation between physicists, medical doctors and radiobiologists will bring the knowledge about low energy photons to the level that is now reached for high energies photons, for the physical data as well as for the radiobiological data.